


Nonlinear anomalous Nernst effect in strained graphene induced by trigonal warpingYing-Li Wu , Ge-Hui Zhu, and Xiao-Qin Yu **School of Physics and Electronics, Hunan University, Changsha 410082, China*

(Received 7 September 2021; revised 3 November 2021; accepted 11 November 2021; published 23 November 2021)

It has recently been reported that a nonlinear anomalous Nernst current (NANC), induced by Berry curvature near the Fermi surface, can be generated as a second-order response to a longitudinal temperature gradient in a wide variety of time-reversal invariant and noncentrosymmetric materials. So far, NANC in two-dimensional Dirac systems has been reported to be finite only in materials with substantial spin-orbit coupling and titled Dirac cones formed from low-energy Dirac quasiparticles. Here, we prove that NANC can also emerge in two-dimensional Dirac materials even in the complete absence of titled Dirac cones and spin-orbit coupling. It's found that the NANC has a quantum origin from the trigonal warping of the Fermi surface. NANC in both trigonal-warping monolayer and bilayer graphene in the presence of uniaxial strain is theoretically investigated. The magnitude of NANC in trigonal-warping bilayer graphene is comparable to those reported which originated from tilted mechanisms in strained MoS₂ and bilayer WTe₂.

DOI: [10.1103/PhysRevB.104.195427](https://doi.org/10.1103/PhysRevB.104.195427)**I. INTRODUCTION**

The Hall (Nernst) effects, referring to a generation of transverse voltage in response to a longitudinal electric field (temperature gradient), represent important paradigms in condensed matter physics [1–3]. Most Hall effects, for example, conventional Hall effect, quantum anomalous Hall effect [4–7], anomalous Hall effect [8–13], and thermal Hall effect [14–18], etc., require time-reversal symmetry broken by a magnetic field or magnetism. The recently discovered nonlinear anomalous Hall effect (NAHE) [19–28] as a second-order response to an electric field, which originates from the dipole moment of Berry curvature in momentum space (namely Berry curvature dipole [19–25]), does not require time-reversal symmetry breaking but inversion symmetry breaking. NAHE has been predicted in a lot of noncentrosymmetric materials, such as two-dimensional (2D) transition-metal dichalcogenides [19,25,26], strained graphene [23], and three-dimensional Weyl semimetals [19,24], etc., and successfully observed in Weyl semimetal WTe₂ [27,28], Dirac semimetal Cd₃As₂ [29], strain monolayer WSe₂ [30], nonmagnetic Weyl-Kondo semimetal Ce₃Bi₄Pd₃ [31], and Weyl semimetal TaIrTe₄ [32]. The NAHE can be generalized to more unconventional responses when the discrete and crystal symmetries are broken and have attracted broad interest in nonlinear anomalous transport phenomena, such as nonlinear spin Hall effect [33,34], the magnus Hall effect [35], magnus thermal Hall effect [36,37], nonlinear thermal Hall effect [38], and the nonlinear anomalous Nernst effect [39].

The nonlinear anomalous Nernst effect (NANE) describes the phenomenon that a nonlinear transverse current can be generated as a second-order response to the longitudinal temperature gradient (Fig. 1) and has a quantum origin arising

from Berry curvature, a local (geometrical) properties of wave function, near the Fermi surface. So far, NANE has been reported in strained MoS₂ [39] and in bilayer WTe₂ [40]. The nonvanishing nonlinear Nernst effect in these materials attributes to substantial spin-orbit coupling and the presence of low-energy Dirac quasiparticles forming titled Dirac cones. Recently, it was reported that nonzero Berry curvature dipoles can emerge in strained graphene [23] in which the spin-orbit coupling and titled Dirac cones are completely absent. It's found the presence of Berry curvature dipole in strained graphene is ascribed to the higher order warping of Fermi surface and gives rise to NAHE. It's natural to ask whether, in the absence of titled Dirac cones and SOC, the warping of the Fermi surface would also give rise to nonzero NANE.

In this paper, we theoretically investigate the NANE in strained graphene with a Fermi surface warping effect. This paper is organized as follows. A pseudovector quantity Λ_d^T , quantizing the nonlinear Nernst current, is recalled and its component along arbitrary direction is derived and determined in Sec. II. The effect of trigonal warping on NANE is analysed for strained monolayer graphene in Sec. III. The behavior of NANE in trigonal-warping bilayer graphene in the presence of uniaxial strain is discussed in Sec. IV. Finally, we give a conclusion in Sec. V.

II. THEORETICAL REVIEW AND DERIVATION

The relation between nonlinear anomalous Nernst current and the Berry curvature near the Fermi surface has been recently determined through the semiclassical framework of the electron dynamics [39,40]. We start out by recalling this relation. When applying a temperature gradient, a nonlinear Nernst current \mathbf{j}_A^{nl} (where the subscript A/ superscript nl refer to anomalous/nonlinear, respectively) in the *a* direction, as the response to second order in temperature gradient, has the

*yuxiaoqin@hnu.edu.cn

form

$$[\mathbf{j}_A^{\text{nl}}]_a = \varepsilon_{abc} \frac{\tau e}{\hbar^2} \partial_b T \partial_d T \Lambda_{cd}^T, \quad (1)$$

with

$$\Lambda_{cd}^T = - \int [d\mathbf{k}] \frac{(E_{\mathbf{k}} - \mu_e)^2}{T^2} \frac{\partial f_0}{\partial k_d} \Omega_c(\mathbf{k}), \quad (2)$$

where $\partial_a = \partial/\partial r_a$, ε_{abc} is the Levi-Civita symbol, $\int [d\mathbf{k}]$ is shorthand for $\int d\mathbf{k}/(2\pi)^d$, τ refers to momentum relaxation time, μ_e represents the chemical potential, \hbar denotes the Planck's constant, $\Omega_c(\mathbf{k})$ indicates the component of Berry curvature in c direction, and $f_0 = (e^{(E_{\mathbf{k}} - \mu_e)/k_B T} + 1)^{-1}$ represents the equilibrium Fermi-Dirac distribution function with k_B indicating Boltzmann constant.

In 2D materials, the Berry curvature Ω is reduced from a pseudovector to a pseudoscalar and only the component vertical to the plane, namely, $\Omega_{c=z}$, is nonzero. The pseudotensorial quantity Λ_{cd}^T , therefore, behaves as a pseudovector contained in the 2D plane:

$$\Lambda_d^T = - \int [d\mathbf{k}] \frac{(E_{\mathbf{k}} - \mu_e)^2}{T^2} \frac{\partial f_0}{\partial k_d} \Omega_z(\mathbf{k}), \quad (3)$$

where $d = x$, or y indicating the component of Λ in d direction. The component of the pseudotensorial quantity Λ_l^T in arbitrary direction $e_l = (\cos\theta, \sin\theta)$, where θ is the azimuthal angle of vector l with respect to the x axis, behaves as a pseudovector contained in the 2D plane that can be determined by

$$\begin{aligned} \Lambda_l^T &= \Lambda_x^T \cos\theta + \Lambda_y^T \sin\theta \\ &= - \int [d\mathbf{k}] \frac{(E_{\mathbf{k}} - \mu_e)^2}{T^2} \frac{\partial f_0}{\partial k_l} \Omega_z(\mathbf{k}). \end{aligned} \quad (4)$$

To obtain the latest line, the relation $\partial f_0/\partial k_l = \cos\theta \partial f_0/\partial k_x + \sin\theta \partial f_0/\partial k_y$ has been used. It should be noted that a symmetry/antisymmetry of an arbitrary function $A(k_l, k_{l_\perp})$ with respect to the $k_{l_\perp} - k_z$ plane, where l_\perp indicates a vector orthogonal to vector l in the 2D plane, corresponds to even/odd parities with respect to arbitrary axis k_l , namely, $A(k_l, k_{l_\perp}) = A(-k_l, k_{l_\perp})/A(k_l, k_{l_\perp}) = -A(-k_l, k_{l_\perp})$. According to Eq. (4), when both energy band $E_{\mathbf{k}}$ and Berry curvature $\Omega_z(\mathbf{k})$ are symmetric with respect to plane $k_{l_\perp} - k_z$, the integrand in Eq. (4) will be odd for Λ_l^T since the partial derivative of Fermi-Dirac distribution function $g_{k_l} = \partial f/\partial k_l \propto \partial E_{\mathbf{k}}/\partial k_l$ will be antisymmetric with respect to plane $k_{l_\perp} - k_z$, namely, $g(k_l, k_{l_\perp}) = -g(-k_l, k_{l_\perp})$, indicating that the quantity $\Lambda_l^T = 0$.

The largest symmetry of a 2D crystal that allows for nonvanishing Λ^T is a single mirror line (a mirror plane that is orthogonal to the 2D crystal). Yu *et al.* [39] have shown that the presence of mirror symmetry accompanying time-reversal symmetry would force the Λ_d^T to be orthogonal to the mirror plane. The current \mathbf{j}_A^{nl} in vector notation can be written as

$$\mathbf{j}_A^{\text{nl}} = \frac{e\tau}{\hbar^2} (\hat{z} \times \nabla T) \nabla T \cdot \Lambda^T. \quad (5)$$

The presence of single mirror symmetry would require that the linear thermally driven transport coefficient tensor has its principal axis aligned with the mirror line. Subsequently, according to Eq. (5), when applying a temperature gradient

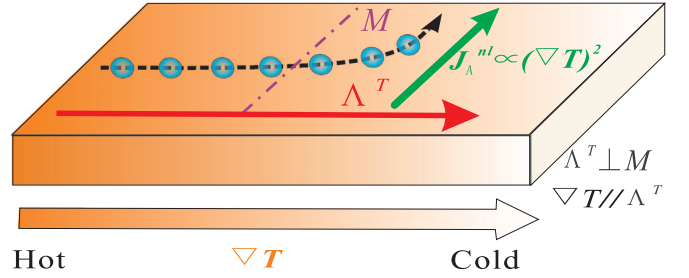


FIG. 1. Schematic illustration of the generation of nonlinear Nernst current j_A^{nl} as a second-order response to the temperature gradient ∇T in two-dimensional materials. The purple dash dot denotes the mirror line. Λ^T is a pseudovector to quantify the nonlinear Nernst effect and is orthogonal to the mirror line.

∇T aligned to Λ^T (orthogonal to the mirror line), all the current flowing vertically to temperature gradient would originate solely from Λ^T (Fig. 1).

III. NONLINEAR ANOMALOUS NERNST EFFECT IN STRAINED TRIGONAL-WARPING MONOLAYER GRAPHENE

The C_{6v} symmetry of a graphene sheet is comprised of a twofold rotation C_2 , a threefold rotation C_3 , and a mirror symmetry. The appearance of these additional symmetries (namely, C_2 symmetry and C_3 symmetry) would force the pseudovector quantity Λ^T to vanish. However, applications of substrate and uniaxial strain can reduce this symmetry and leave only a single mirror operation, in which the nonlinear Hall effect would be observed. In fact, when placing the graphene sheet on the substrate, for example, lattice-matched h-BN [41], a staggered chemical potential Δ (Semeoff mass [42]) between the two honeycomb sublattices will be generated and the inversion symmetry will be broken, resulting in symmetry reduction of graphene from C_{6v} symmetry to C_{3v} symmetry. The C_{3v} symmetry can be further reduced to leave only mirror symmetry through applying a uniform uniaxial strain to the honeycomb lattice along one of the two main crystallographic directions.

In previous works, the nonvanishing nonlinear Nernst effect has been shown to originate from the tilt mechanism (namely, the contribution from a term $\propto \tau k_x \sigma_0$) in materials with substantial spin-orbit coupling. In the following, we will show that the warping effect of the Fermi surface can also give rise to a finite nonlinear Nernst effect instead of tilt mechanism. Taking into account the trigonal warping to the k^2 term, the effective Hamiltonian of monolayer graphene to the second order in momentum and the first order in strain is

$$\hat{H}_{\text{warped}}^{\text{ml}} = M_1(\mathbf{k})\hat{\sigma}_x + M_2(\mathbf{k})\hat{\sigma}_y + \frac{\Delta}{2}\hat{\sigma}_z, \quad (6)$$

with

$$\begin{aligned} M_1(\mathbf{k}) &= \tau_v v_x k_x + \lambda_1 k_y^2 - \lambda_2 k_x^2, \\ M_2(\mathbf{k}) &= v_y k_y + 2\tau_v \lambda_3 k_x k_y, \end{aligned} \quad (7)$$

where the subscript ml refers to monolayer, $\tau_v (= \pm 1)$ is the valley index, $\hat{\sigma}$ represents the Pauli matrices for the two basis functions of energy band, Δ refers to Semenoff mass,

$v_x = v_F[1 - \beta(3u_{xx} + u_{yy})/4]$ and $v_y = v_F[1 - \beta(u_{xx} + 3u_{yy})/4]$ are two strain-dependent Fermi velocities and depend on the strain tensor u_{xx} and u_{yy} , $\lambda_{1,2,3}$ are the warping related parameters which, in general, are not equivalent when considering strain-momentum coupling terms, and determined through $\lambda_1 = \lambda_3 = \lambda_0[1 - \beta(3u_{xx} + u_{yy})/4]$ and $\lambda_2 = \lambda_0[1 - \beta(5u_{yy} - u_{xx})/4]$, where β is a materials-dependent parameter (in graphene $\beta \approx 2$). The energy eigenvalues are

$$E_{\tau_v,n}^{\text{ml}}(\mathbf{k}) = n\sqrt{\frac{\Delta^2}{4} + M_1^2(\mathbf{k}) + M_2^2(\mathbf{k})}, \quad (8)$$

where n is the band index. The Berry curvature is determined by $\Omega_n(\mathbf{k}) = \hat{\mathbf{z}} \cdot \nabla_{\mathbf{k}} \times \langle \Psi_n | i \nabla_{\mathbf{k}} | \Psi_n \rangle$ for 2D materials, where $\nabla_{\mathbf{k}}$ means directional derivatives with respect to the momentum \mathbf{k} , and Ψ_n is the eigenstate of the Hamiltonian. For the effective Hamiltonian in Eq. (6), the Berry curvature is

$$\Omega_{\tau_v,n}^{\text{ml}}(\mathbf{k}) = -n \frac{\Delta(\partial_{k_x} M_1 \partial_{k_y} M_2 - \partial_{k_y} M_1 \partial_{k_x} M_2)}{4\left(\sqrt{\frac{\Delta^2}{4} + M_1^2 + M_2^2}\right)^3}, \quad (9)$$

where ∂_{k_j} is the shorthand for $\partial/\partial k_j$ ($j = x, y$) and the variable \mathbf{k} in bracket of $M_{i=1,2}(\mathbf{k})$ has been neglected for simplification. The energy (Berry curvature) at the two valleys takes same (opposite) values when reversing k_x value, namely, $E_K(k_x, k_y) = E_{-K}(-k_x, k_y)$ and $\Omega_K(k_x, k_y) = -\Omega_{-K}(-k_x, k_y)$ (Fig. 6), respectively, which is entailed by time-reversal symmetry. Hence $g_{\tau_v}(\mathbf{k}) = \partial f_0/\partial k_x \propto \partial E_{\tau_v}/\partial k_x$ has opposite signs on the opposite side of Fermi energy for different valleys, namely, $g_K(k_x, k_y) = -g_{-K}(-k_x, k_y)$. Therefore, Λ_x^T from different valleys has the same sign and contribute additively, resulting in the total Λ_x^T . In the following, therefore, we will only analyze the Λ_x^T from the K valley for simplification and the total Λ_x^T is obtained by multiplying 4 (considering both valley and spin contribution).

As illustrated in Figs. 2(a) and 2(c), in the absence of trigonal warping effect (i.e., $\lambda_0 = 0$), although the shapes of the energy band and Berry curvature for the K valley are distorted by uniaxial tensile strain or compressive strain, the symmetries of the energy band and Berry curvature with respect to the $k_{d\perp} - k_z$ plane (where $d = x$ or y) are still guaranteed, which hints $\Lambda_x^T = 0$ and $\Lambda_y^T = 0$ (for details, see Sec. II), indicating the vanishing nonlinear Nernst effect in the absence of trigonal warping effect.

In the presence of trigonal warping effect but without strain, both the Fermi surface and Berry curvature for the K valley become trigonal-like [the green line in Figs. 2(b) and 2(d)] from the circle [the green line in Figs. 2(a) and 2(c)] and are invariant under the following two operators: (1) mirror reflection M_{k_y} about the $k_x - k_z$ plane, and (2) threefold rotation C_3 about the k_z axis, which hints that both of the energy band $E_{\mathbf{k}}$ and Berry curvature $\Omega(\mathbf{k})$ are symmetric with respect to plane $k_l - k_z$ (where $k_l = k_x, C_3 k_x$, and $C_3^2 k_x$). Thus, we can have $\Lambda_y^T = 0$, $\Lambda_{C_3 y}^T = 0$ and $\Lambda_{C_3^2 y}^T = 0$ (see details in Sec. II).

Accompanying with the equality $\Lambda_{C_3 y}^T = -\Lambda_x^T/2 + \sqrt{3}\Lambda_y^T/2$ [Eq. (4)], one can also have $\Lambda_x^T = 0$. Therefore, in the absence of strain, there is also no nonlinear current generated vertically to the temperature gradient regardless of the direction of applied temperature gradient.

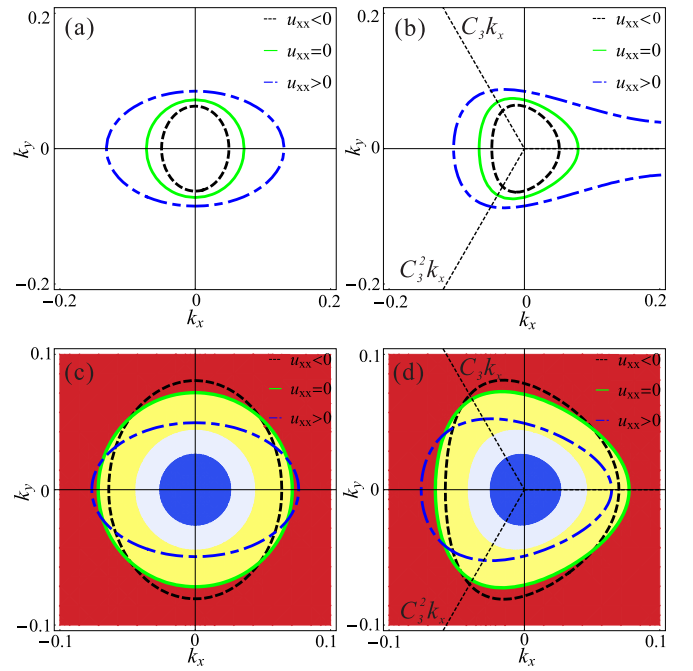


FIG. 2. Schematic of energy contour [(a), (b)] and Berry curvature [(c), (d)] of the conduction band for K valley with or without tensile (compressive) strain for non-trigonal-warping monolayer graphene [(a), (c)] and trigonal-warping monolayer graphene [(b), (d)], respectively. The blue dash dot line (black dash line) and the green solid line indicate energy band or Berry curvature with uniaxial tensile (compressive) strain and without strain, respectively. All lines are the same energy. The color background in (c) and (d) represent the Berry curvature of non-trigonal-warping monolayer graphene. Momenta are measured in units of the inverse of the lattice constant a .

Hence, it's evident that both trigonal warping effect and strain are necessary conditions to produce nonvanishing Λ_x^T for monolayer graphene. Once applying uniaxial tensile/compressive strain u_{xx} along zigzag direction (x direction), the trigonal-like shape of energy band and Berry curvature will be stretched/compressed along k_x direction [Figs. 2(b) and 2(d)]. It's obvious that the threefold rotation C_3 about k_z is broken by strain but the mirror symmetry M_{k_y} is still survived [Figs. 2(b) and 2(d)], indicating that the y component of quantity Λ^T could still be zero but the x component could no longer be zero.

Figures 3(a) and 3(b) show the dependence of quantity Λ_x^T on the Fermi energy and strain. It's interesting to point out that although the maximum of the Berry curvature appears at the Dirac point, the signal of Λ_x^T is almost zero at Dirac point in low temperature. This nearly disappearing signal of Λ_x^T at the Dirac point can be understood as follows: when the Fermi energy gets close to the Dirac point ($E - \Delta/2 = 0$ eV), the Fermi surface manifests itself as a circle and the trigonal warping is not apparent [Figs. 6(a) and 6(b)], resulting in an almost vanishing nonlinear anomalous effect. Modulating the Fermi energy through gate voltage to an appropriate value, the signal of Λ_x^T can reach its maximum [Fig. 3(a)]. The appearance of the peak in Fig. 3(a) can be qualitatively attributed to the joint result of Berry curvature and trigonal warping

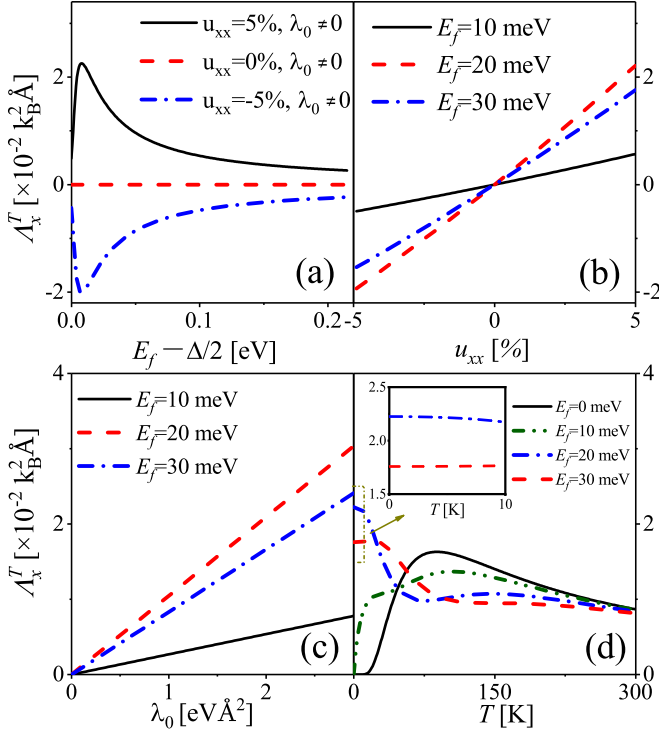


FIG. 3. The quantity Λ_x^T dependent on Fermi energy E_F , strain parameter u_{xx} , trigonal warping parameters λ_0 , and temperature T . (a) Λ_x^T versus E_F with and without tensile (compressive) strain. (b) Λ_x^T versus u_{xx} for different Fermi energies. (c) Λ_x^T versus λ_0 for different Fermi energies. (d) Quantity Λ_x^T versus T for different Fermi energies. The temperatures in (a)–(c) are taken at 5 K. $u_{xx} = 5\%$ is fixed in (b)–(d). The trigonal warping parameters λ_0 is $2.118 \text{ \AA}^2 \times \text{eV}$ in (a), (b), and (d). The Semenoff mass is taken as 20 meV.

effect. Increasing the value of Fermi energy E_F , the Berry curvature will decrease, which tends to weaken the signal of nonlinear anomalous Nernst effect and the Fermi surface, on the other hand, will start to deviate from circle and become more trigonal-like (Fig. 6), namely, the trigonal warping effect gradually becomes more profound which tends to give rise to enhancement of nonlinear anomalous Nernst effect in presence of strain. The combination of these two factors leads to the signal of Λ_x^T that increases rapidly first and then gradually decreases due to the decrease of Berry curvature, giving rise to a peak feature.

The quantity Λ_x^T shows linear dependence on the strain parameters u_{xx} [Fig. 3(b)] and undergoes a sign change when modulating the tensile strain into compressive strain. The temperature T dependence of Λ_x^T at different Fermi energy levels is shown in Fig. 3(d). As expected, when the Fermi energy is located in the gap ($E_F = 0$ meV) or the bottom of the conduction band ($E_F = 10$ meV), the nonlinear anomalous Nernst effect tends to be zero when T approaches zero since there is no charge carriers. However, when modulating the Fermi energy to the conduction band ($E_F > 10$ meV), Λ_x^T tends to be a constant when the temperature approaches zero (see Appendix B for a detailed discussion). When the Fermi energy is located in the gap or the bottom of the conduction band, with the temperature increasing, the quantity Λ_x^T increases first,

owing to the thermal broadening effect of the nonequilibrium Fermi distribution and then decreases gradually due to the factor $1/T^2$ appearing in Eq. (3).

IV. NONLINEAR ANOMALOUS NERNST EFFECT IN STRAINED TRIGONAL-WARPING BILAYER GRAPHENE

Having investigated the nonlinear Nernst effect in uniaxially strained trigonal-warping monolayer graphene, we now study the nonlinear Nernst effect in bilayer graphene in the (AB) Bernal-stacked structure. The inversion symmetry of bilayer graphene can be broken through applying an external electric field perpendicular to the layers. The applied electric field actually induces a spectral gap Δ and reduces the point-group symmetry from D_{3d} to C_{3v} . Like monolayer graphene, point group C_{3v} can be further reduced to C_v with the additional application of a uniaxial strain, resulting in a nonvanishing quantity Λ^T . In the presence of uniaxial strain, the strain-dependent Hamiltonian of bilayer graphene [43,44] can be written as

$$\begin{aligned} \hat{H}_{\text{warped}}^{\text{bl}} &= \tau_v \frac{\Delta}{2} \hat{\sigma}_z + \left(-\frac{\hbar^2(k_x^2 - k_y^2)}{2m} + w \right) \hat{\sigma}_x \\ &\quad - \frac{\hbar^2 k_x k_y}{m} \hat{\sigma}_y + \hat{h}_w, \\ \hat{h}_w &= \tau_v v_3 \hbar k_x \hat{\sigma}_x - \tau_v v_3 \hbar k_y \hat{\sigma}_y, \end{aligned} \quad (10)$$

where \hat{h}_w comes from the skew hopping between the layers and introduces a triangular distortion of Fermi circle around $K/(-K)$ point [Fig. 4(d)], namely, trigonal warping, v_3 represents the Fermi velocity related to the skew hopping between the layers, the effect of strain is involved through term $w = \frac{3}{4} \gamma_3 (u_{xx} - u_{yy})(\beta_3 - \beta_0)$, with $\gamma_3 \approx 0.3$, $\beta_0 \approx 2.18$ and $\beta_3 \approx 0.21$ for bilayer graphene [44], m denotes an effective mass directly dependent on the interlayer coupling, and $\hat{\sigma}_{i=x,y,z}$ is Pauli matrix for sublattice A/B. It should be noted that the wave function Φ describing amplitude on A and B sites is $(\phi(A), \phi(B))$ in valley K ($\tau_v = +1$), whereas in valley $-K$ ($\tau_v = -1$), the order of components are reversed, namely, $\Phi_{\tau_v=-1} = (\phi(B), \phi(A))$, which can actually explain the appearance of valley index τ_v in the term $\tau_v \Delta \sigma_z / 2$. The energy band and Berry curvature are found to be

$$E_{\tau_v, n}^{\text{bl}}(\mathbf{k}) = n \sqrt{\frac{\Delta^2}{4} + N_1^2(\mathbf{k}) + N_2^2(\mathbf{k})}, \quad (11)$$

$$\Omega_{\tau_v, n}^{\text{bl}}(\mathbf{k}) = -\tau_v n \frac{\Delta \left(\frac{\hbar^4(k_x^2 + k_y^2)}{m^2} - v_3^2 \hbar^2 \right)}{4 \left(\sqrt{\frac{\Delta^2}{4} + N_1^2 + N_2^2} \right)^3}, \quad (12)$$

where $N_1(\mathbf{k}) = -\frac{\hbar^2(k_x^2 - k_y^2)}{2m} + \tau_v v_3 \hbar k_x + w$, $N_2(\mathbf{k}) = -\frac{\hbar^2 k_x k_y}{m} - \tau_v v_3 \hbar k_y$, and the subscript bl in $E_{\tau_v, n}^{\text{bl}}(\mathbf{k})$ and $\Omega_{\tau_v, n}^{\text{bl}}(\mathbf{k})$ refers to bilayer. Being analogous to monolayer graphene, the Λ_x^T from both valleys will have the same sign and magnitude guaranteed by time-reversal symmetry (see details in Sec. III). Thus, the NANE from the K valley will be analyzed for simplicity in the following whereas the final magnitude of Λ_x^T will include the contributions from both valley and spin through multiplying 4. In the absence of the

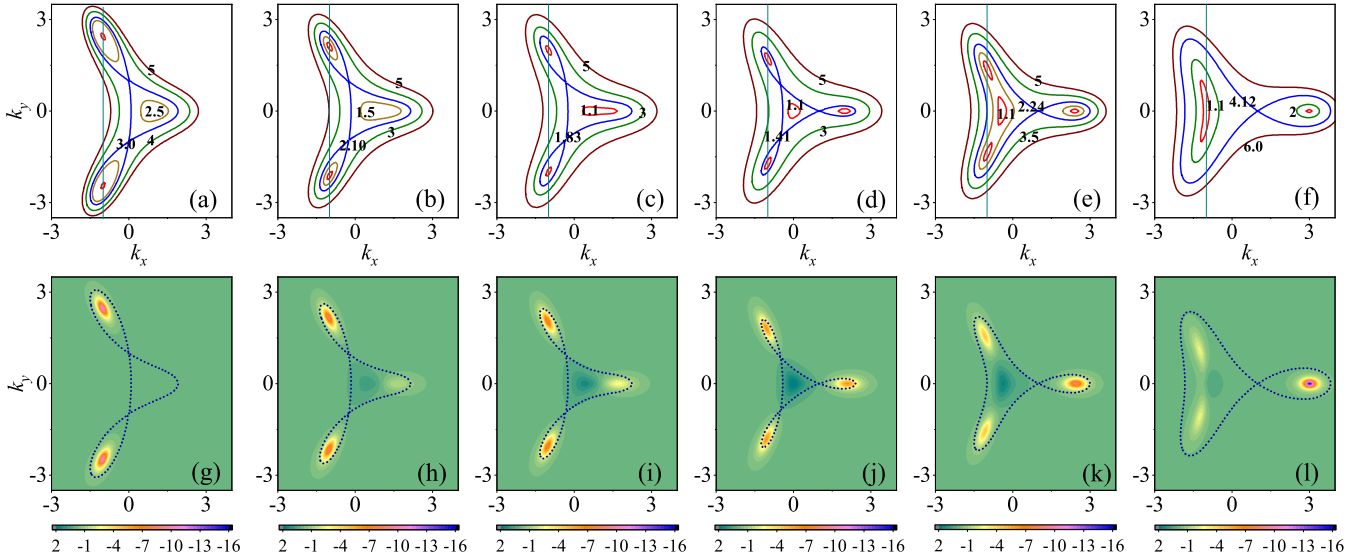


FIG. 4. Schematic of energy contour and Berry curvature Ω of the conduction band for K valley of trigonal-warping bilayer graphene: $w = -3\varepsilon_L$ [(a), (g)], $w = -1.5\varepsilon_L$ [(b), (h)], $w = -\varepsilon_L$ [(c), (i)], $w = 0\varepsilon_L$ [(d), (j)], $w = 1\varepsilon_L$ [(e), (k)], and $w = 3\varepsilon_L$ [(f), (l)]. The dashed lines in (g)–(l) describe the Fermi surface at which the Lifshitz transition happens. The vertical line located in $k_x = -1$ is a reference line to show the shift of the left two Dirac point for $w \leq 3$ and disappearance of left two Dirac cones for $w > 3$. The gap Δ is fixed at 2 meV. Momenta are measured in units of k_L and the energies are measured in units of ε_L , respectively.

trigonal effect (namely, $v_3 = 0$), both energy contour and Berry curvature are symmetric under the exchange $k_y \rightarrow -k_y$ (or $k_x \rightarrow -k_x$), hinting the vanishing nonlinear Nernst effect.

Figure 4 illustrates the energy contour and Berry curvature of trigonal-warping bilayer graphene at different values of strain in the absence of inversion symmetry ($\Delta \neq 0$). It's easy to observe that the strain-free ($w = 0$) bilayer graphene [Fig. 4(d)] features a Lifshitz transition at energy $1.41\varepsilon_L$ (where $\varepsilon_L = mv_3^2/2 \approx 1$ meV), in which the Fermi surface splits from a single connected pocket into four different ones as the energy and momentum are decreased: the electronic dispersion consists of one central Dirac cone located at the K ($-K$) point of the Brillouin zone and three leg Dirac cones. A characteristic momentum $k_L = mv_3/\hbar (\approx 0.035 \text{ nm}^{-1})$ can be defined through the distance between the different cones. In the presence of the strain [Figs. 4(a)–4(c) and 4(e)–4(f)], not only do the Dirac cones move from their unstrained positions but the topology of Fermi surface changes through merging the cones together. For $-\varepsilon_L < w \leq 3\varepsilon_L$, there are always four Dirac points, two located at $k_L(1 \pm \sqrt{1 + w/\varepsilon_L}, 0)$ along the k_x axis in the Brillouin zone and the remaining two at $k_L(-1, \pm\sqrt{3 - w/\varepsilon_L})$. At $w = -\varepsilon_L$, the two Dirac cones in the k_x axis merge into a point $k_L(1, 0)$, bringing about a local minimum with $E = \sqrt{2/4 + (1 + w/\varepsilon_L)^2}$ in the dispersion relation which survives until $w \geq -9\varepsilon_L$. For $w > 3\varepsilon_L$, instead, the two leg Dirac cones located at $k_L(-1, \pm\sqrt{3 - w/\varepsilon_L})$ will disappear and only the cones in the k_x axis are survived. The rich fermiologies of bilayer graphene induced by strain can also be visible in the plots of Berry curvature [Figs. 4(g)–4(l)].

One can notice that the plots of energy and Berry curvature [Fig. 4] are symmetric with respect to plane $k_x - k_y$ guaranteed by the combination time-reversal symmetry and mirror symmetry, hinting that $\Lambda_y^T = 0$ (see details in Sec. II). In the absence of strain, the nonlinear Nernst coefficient Λ_x^T will also be zero, which is constrained by the threefold C_3 rotation

symmetry. However, It should be note that while the central Dirac cone has a disappearing Λ_x^T like the unstrained trigonal-warping monolayer graphene, the three leg Dirac cones do have a nonzero Λ_x^T when counting by themselves. The perfect cancellation of these three nonzero contributions to Λ_x^T is lost in the presence of uniaxial strain owing to the breaking of threefold rotation symmetry by strain. Moreover, in the presence of finite uniaxial tensile (compressive) strain, shapes of the energy and Berry curvature of the central Dirac cone will be stretched/compressed and lead to a nonzero contribution to Λ_x^T . Therefore, the presence of uniaxial tensile will give rise to a net nonlinear Nernst coefficient Λ_x^T [Fig. 5] due to the deformation of the cones of the trigonal-warping bilayer graphene.

The deformation of Dirac cones and the rich fermiology of the trigonal-warping bilayer graphene give rise to the richer features of Λ_x^T dependent on the Fermi energy E_F and the strain w than the trigonal-warping monolayer graphene as shown in Figs. 5(a), 4(c), and 5(d). The sign of Λ_x^T is no longer simply dependent on the properties of strain (namely, tensile strain or compressive strain). When fixing the Fermi energy, the sign of Λ_x^T would also be changed by varying the magnitude of compressive strain ($w < 0$) [Fig. 5(a)]. Besides, when tuning the compressive strain to the appropriate value, one would also reverse the sign of the Λ_x^T by modulating the Fermi energy through gate voltage [Fig. 5(b)], thus inverting the direction of the generated transverse current when applying temperature gradient. It's interesting to point out that although the nonvanishing signal of Λ_x^T in trigonal-warping bilayer graphene only appears near the bottom of conduction band with a few meV, the maximum of Λ_x^T for $\Delta = 2$ meV at $w = 3\varepsilon_L$ (corresponding roughly to $u_{xx} = 0.6\%$ strain) reaches $100 k_B^2 \text{ \AA}$, which is four orders larger than that of monolayer graphene. It should be mentioned that the magnitude of Λ_x^T in bilayer graphene can be further enlarged by decreasing Δ

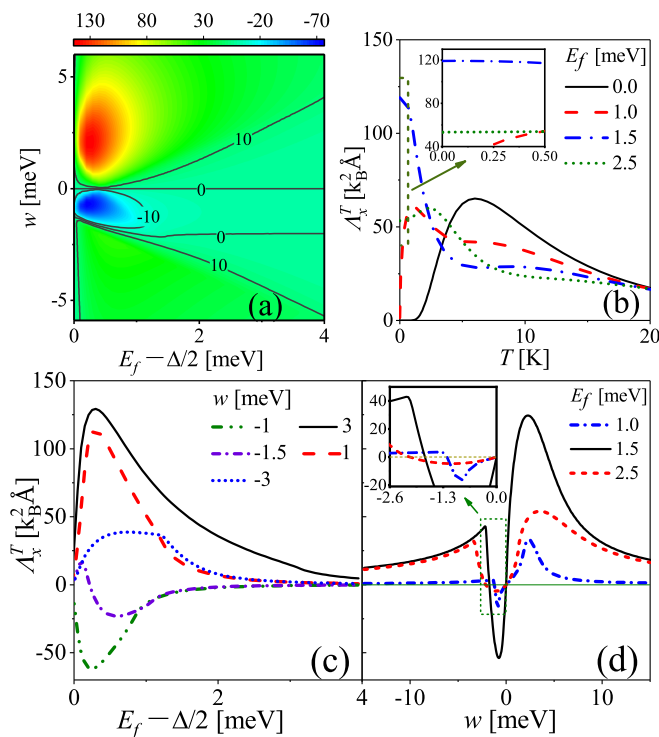


FIG. 5. (a) The quantity Λ_x^T as a function of Fermi energy E_F and strain parameter w . (b) The quantity Λ_x^T versus T for different Fermi energies. (c) The quantity Λ_x^T versus E_F for different w 's. (d) The quantity Λ_x^T versus w for the selective Fermi energy. Momenta are measured in units of k_L . $T = 0.1$ K is fixed in (c) and (d). $w = 3$ meV is taken in (b). Parameter used: $\Delta = 2$ meV.

and reach almost $500 k_B^2 \text{ \AA}$ for $\Delta = 0.25$ meV (Fig. 7). The early reported Λ_x^T , stemmed from tilted Dirac cones, ranges from -10 to $10 k_B^2 \text{ \AA}$ at 20 K for bilayer WS_2 [40] and is in the range of $0.001 - 1000 k_B^2 \text{ \AA}$ for MoS_2 [39]. Therefore, the magnitude of Λ_x^T in trigonal-warping bilayer graphene is comparable to those originated from tilted Dirac cones. The temperature dependence of Λ_x^T in bilayer graphene is similar to that in monolayer graphene. When locating Fermi energy in the conduction band, the quantity Λ_x^T will tend to be a constant as T approaching zero.

When applying the temperature gradient in the x direction, the nonlinear anomalous Nernst current is found to be $j_{A,y}^{\text{nl}} = e\tau\Lambda_x^T(\nabla_x T)^2/\hbar^2$ [Eq. (5)], which corresponds to a voltage drop $\Delta V_{\text{NANE}} = w j_y/\sigma = (\tau/\sigma) \times e w \Lambda_x^T (\nabla_x T)^2/\hbar^2$ in the open-circuit case. To numerically estimate the signal of NANE in bilayer graphene, we use the following typical values: $ek_B^2/\hbar^2 \approx 2.215 \text{ nA/K}^{-2}\text{ps}$, $\Lambda_x^T \approx 500 k_B^2 \text{ \AA}$ [Fig. 7(a)] taken for $\Delta = 0.25$ meV, and the ratio τ/σ is estimated by $\tau/\sigma = m/(n_c e^2)$, because the scattering relaxation time τ can be estimated by m/e^2 and the conductivity σ is determined through $n_c \mu e$. The effective mass m for bilayer graphene is $0.037 m_e$ [45]. The carrier density n_c near the bottom of conduction band ranges from 10^8 to 10^{11} cm^{-2} when varying the gap value Δ [23]. We use $n_c \sim 10^9 \text{ cm}^{-2}$ for $\Delta = 0.25$ meV. In experiments, the temperature gradient can already reach $1.5 \text{ K}\mu\text{m}^{-1}$ [46]. Thus, a voltage drop ΔV_{NANE} generated from

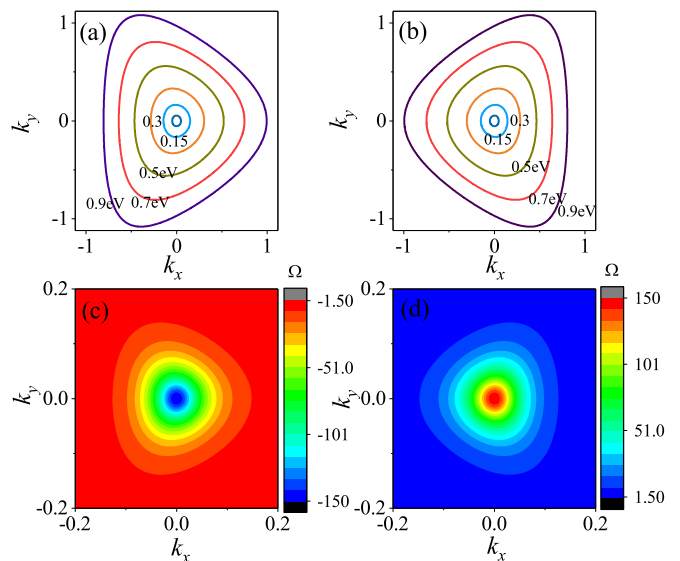


FIG. 6. Schematic of energy contour E_n [(a), (b)] and Berry curvature Ω_n [(c), (d)] of the conduction band for K and $-K$ valley for trigonal-warping monolayer graphene in presence of uniaxial strain, respectively. Momenta are measured in units of the inverse of the lattice constant a , and Berry Curvature measured in units of a^2 .

nonlinear anomalous Nernst effect can reach 2 mV with the width of sample $w = 50 \mu\text{m}$, which is measurable [47].

V. CONCLUSION

In summary, we have shown that a nonzero nonlinear Nernst current would be generated as a second-order response to temperature gradient even in the complete absence of tilted Dirac cones and spin-orbit coupling in 2D materials as a result of the trigonal effect. The nonlinear Nernst effect in trigonal-warping monolayer and bilayer graphene in the presence of uniaxial strain have been theoretically and systematically investigated. In bilayer graphene, the nonlinear Nernst effect is strongly enhanced and the quantity Λ_x^T quantifying the nonlinear Nernst effect is comparable to those reported in strained

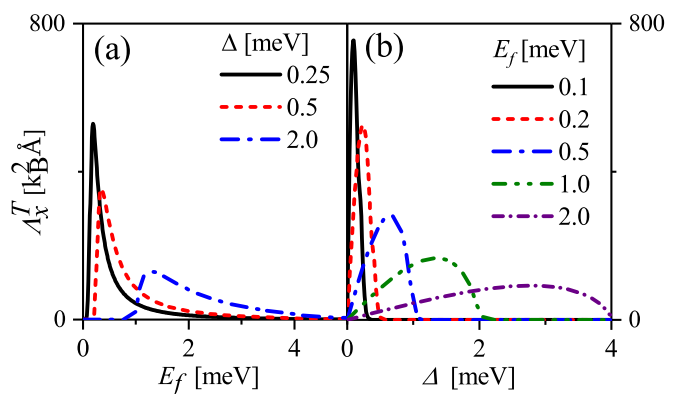


FIG. 7. (a) The quantity Λ_x^T as a function of Fermi energy for different gaps Δ in bilayer graphene. (b) The quantity Λ_x^T as a function of Fermi energy for different gaps Δ . Parameter used: $T = 0.1$ K and $w = 3$ meV.

MoS₂ and bilayer WS₂ which originated from tilted Dirac cones. The study shows that both trigonal warping effect and uniaxial strain are necessary conditions to produce nonvanishing Λ^T in both monolayer and bilayer graphene. Λ_x^T shows linear dependence on strain in monolayer graphene but manifests itself a nonmonotonical dependence on strain in bilayer graphene due to the rich fermiology of the trigonal-warping bilayer. It's interesting to point out that when Fermi energy is located in the conduction band, Λ_x^T extends to be a constant in both bilayer and monolayer graphene as the temperature approaches zero.

ACKNOWLEDGMENTS

This work is supported by the Fundamental Research Funds for the Central Universities and the NSFC (Grant No. 12004107).

APPENDIX A: THE SAME CONTRIBUTION TO Λ_d^T FROM DIFFERENT VALLEYS IN MONOLAYER GRAPHENE

The quantity Λ_d^T characterizing the nonlinear Nernst effect from τ_v valley for graphene in conduction band is given as

$$\Lambda_{d,\tau_v}^T = -2 \int [d\mathbf{k}] \frac{(E_{\tau_v}(\mathbf{k}) - \mu_e)^2}{T^2} \frac{\partial f_0}{\partial k_d} \Omega_{\tau_v}(\mathbf{k}), \quad (\text{A1})$$

where 2 is for spin and $\tau_v, \pm 1$ denotes valley index with $\tau_v = +1(-1)$ for $K(-K)$ valley, respectively. Figure 6 illustrates the energy band and Berry curvature of monolayer graphene with strain and hexagonal warping effect. One can easily observe that $E_K(k_x, k_y) = E_{-K}(-k_x, k_y)$ and $\Omega_K(k_x, k_y) = -\Omega_{-K}(-k_x, k_y)$, which is entailed by time-reversal symmetry. Therefore, $g_{\tau_v}(\mathbf{k}) = \partial f_0 / \partial k_x \propto \partial E_{\tau_v} / \partial k_x$ has opposite signs on the opposite side of Fermi energy for different valleys, namely, $g_K(k_x, k_y) = -g_{-K}(-k_x, k_y)$. Therefore, Λ_x^T from different valleys has the same sign and contributes additively, resulting in the total Λ_x^T .

APPENDIX B: SOMMERFELD EXPANSION

In this Appendix, we apply the Sommerfeld expansion to investigate the temperature dependence of Λ_d^T at low temperature. The evaluation of integrals of the form

$$A(T, E_F) = - \int dE \frac{\partial f(E)}{\partial E} H(E), \quad (\text{B1})$$

where $f(E) = (e^{(E-E_F)/k_B T} + 1)^{-1}$ represents the Fermi-Dirac distribution function and $H(E)$ is a general function of E , can be done approximately with the Sommerfeld expansion

$$A(T, E_F) \simeq H(E_F) + \frac{\pi^2}{6} (k_B T)^2 H^{(2)}(E_F) + \frac{7\pi^4}{360} (k_B T)^4 H^{(4)}(E_F) + O(T^4), \quad (\text{B2})$$

where $H^{(n)}$ denotes the n th derivative of $H(E)$ with respect to E evaluated at $E = E_F$. The expression for pseudovector Λ_{cd}^T in Eq. (2) can be rewritten as

$$\begin{aligned} \Lambda_{cd}^T &= -\frac{1}{T^2} \int [d\mathbf{k}] (E_{\mathbf{k}} - E_F)^2 \Omega_{\mathbf{k},c} \frac{\partial f_0}{\partial k_d} \\ &= - \int dE G(E) \frac{\partial f_0}{\partial E}, \end{aligned} \quad (\text{B3})$$

with

$$G(E) = \frac{(E - E_F)^2}{T^2} \int [d\mathbf{k}] \delta(E - E_{\mathbf{k}}) \Omega_{\mathbf{k},c} \frac{\partial E_{\mathbf{k}}}{\partial k_d}. \quad (\text{B4})$$

Applying Eq. (B2), the pseudovector Λ_{cd}^T is found to be

$$\Lambda_{cd}^T = \frac{\pi^2 k_B^2}{3} G_2(E_F) + \frac{7\pi^4 k_B^4}{60} T^2 G_2^{(2)}(E_F) + O(T^4), \quad (\text{B5})$$

where

$$G_2(E) = \int [d\mathbf{k}] \delta(E - E_{\mathbf{k}}) \Omega_{\mathbf{k},c} \frac{\partial E_{\mathbf{k}}}{\partial k_d}. \quad (\text{B6})$$

It should be noted that when the Fermi energy E_F is located in the gap, $G_2(E_F)$ will equal zero since there is no energy state to carry electrons. According to Eqs. (B5) and (B6), consequently, the pseudovector Λ_{cd}^T tends to be a constant [$\propto G_2(E_F)$] at low temperature and is independent of the temperature gradient when the Fermi energy is located in the conduction band or the valence band.

APPENDIX C: THE GAP DEPENDENCE OF QUANTITY Λ_x^T FOR BILAYER GRAPHENE

Figure 7(a) displays the gap dependence of the quantity Λ_x^T as a function of Fermi energy. The maximum value of quantity Λ_x^T is enlarged by decreasing the value of gap Δ [Fig. 7(a)]. Figure 7(b) illustrates the variation of Λ_x^T versus Δ . When increasing Δ value, the quantity Λ_x^T increases first and then decreases, giving rise to a peak feature. The appearance of the peak feature in Fig. 7(b) might be explained as follows: (a) The quantity Λ_x^T quantifying NANC stems from the Berry curvature near the Fermi level. (b) The maximum of Berry curvature appears at Dirac point or the bottom of the conduction band (namely, $E = \Delta/2$). (c) When increasing the value Δ , the bottom of the conduction band will first get close to the fixed Fermi level, giving an enhancement of Λ_x^T , and then get away from the Fermi level, leading to a decrease of Λ_x^T and further the peak feature.

In addition, it's found that at a lower Fermi energy, the value of the peak becomes larger and the position of the peak appears at smaller Δ [Fig. 7(b)]. The appearance of such large Λ_x^T at small Δ might be attributed to the enhanced Berry curvature. Decreasing the value of Δ , the Berry curvature will be increased, which tends to strengthen the signal of nonlinear anomalous Nernst effect.

[1] E. H. Hall, *Am. J. Math.* **2**, 287 (1879).

[2] R. Karplus and J. M. Luttinger, *Phys. Rev.* **95**, 1154 (1954).

[3] K. V. Klitzing, G. Dorda, and M. Pepper, *Phys. Rev. Lett.* **45**, 494 (1980).

[4] C.-Z. Chang, J. Zhang, X. Feng, J. Shen, Z. Zhang, M. Guo, K. Li, Y. Ou, P. Wei, L. L. Wang, Z. Q. Ji, Y. Feng, S. Ji, X. Chen, J. Jia, X. Dai, Z. Fang, S. C. Zhang, K. He, Y. Wang *et al.* *Science* **340**, 167 (2013).

[5] M. Onoda and N. Nagaosa, *Phys. Rev. Lett.* **90**, 206601 (2003).

- [6] Z. Qiao, S. A. Yang, W. Feng, W. K. Tes, J. Ding, Y. Yao, J. Wang, and Q. Niu, *Phys. Rev. B* **82**, 161414(R) (2010).
- [7] G. Xu, H. M. Weng, Z. J. wang, X. Dai, and Z. Fang, *Phys. Rev. Lett.* **107**, 186806 (2011).
- [8] A. A. Burkov, *Phys. Rev. Lett.* **113**, 187202 (2014).
- [9] H. Chen, Q. Niu, and A. H. MacDonald, *Phys. Rev. Lett.* **112**, 017205 (2014).
- [10] N. Kiyohara, T. Tomita, and S. Nakatsuji, *Phys. Rev. Appl.* **5**, 064009 (2016).
- [11] A. J. Bestwick, E. J. Fox, X. F. Kou, L. Pan, K. L. Wang, and D. Goldhaber-Gordon, *Phys. Rev. Lett.* **114**, 187201 (2015).
- [12] M. Blinov, A. Aryal, S. Pandey, I. Dubenko, S. Talapatra, V. Prudnikov, E. Lahderanta, S. Stadler, V. Buchelnikov, V. Sokolovskiy, M. Zagrebin, A. Granovsky, and N. Ali, *Phys. Rev. B* **101**, 094423 (2020).
- [13] N. N. Zhao, K. Liu, and Z. Y. Lu, *Phys. Rev. B* **103**, 205104 (2021).
- [14] A. Freimuth and B. Zeini, *Phys. Rev. B* **67**, 052504 (2003).
- [15] M. Stone, *Phys. Rev. B* **85**, 184503 (2012).
- [16] A. Gromov and A. G. Abanov, *Phys. Rev. Lett.* **114**, 016802 (2015).
- [17] K. Sugii, M. Shimosawa, D. Watanabe, Y. Suzuki, M. Halim, M. Kimata, Y. Matsumoto, S. Nakatsuji, and M. Yamashita, *Phys. Rev. Lett.* **118**, 145902 (2017).
- [18] C. M. Varma, *Phys. Rev. B* **102**, 075113 (2020).
- [19] I. Sodemann and L. Fu, *Phys. Rev. Lett.* **115**, 216806 (2015).
- [20] T. Low, Y. Jiang, and F. Guinea, *Phys. Rev. B* **92**, 235447 (2015).
- [21] Z. Z. Du, C. M. Wang, H.-Z. Lu, and X. C. Xie, *Phys. Rev. Lett.* **121**, 266601 (2018).
- [22] Z. Z. Du, C. M. Wang, Shuai Li, Hai-Zhou Lu, X. C. Xie, *Nat. Commun.* **10**, 3047 (2019).
- [23] R. Battilomo, N. Scopigno, and C. Ortix, *Phys. Rev. Lett.* **123**, 196403 (2019).
- [24] J. I. Facio, D. Efremov, K. Koepf, J.-S. You, I. Sodemann, and J. van den Brink, *Phys. Rev. Lett.* **121**, 246403 (2018).
- [25] J.-S. You, S. Fang, S.-Y. Xu, E. Kaxiras, and T. Low, *Phys. Rev. B* **98**, 121109(R) (2018).
- [26] Y. Zhang, Y. Sun, and B. Yan, *Phys. Rev. B* **97**, 041101(R) (2018).
- [27] Q. Ma, S.-Y. Xu, H. Shen, D. MacNeill, V. Fatemi, T.-R. Chang, A. M. M. Valdivia, S. Wu, Z. Du, C.-H. Hsu, S. Fang, Q. D. Gibson, K. Watanabe, T. Taniguchi, R. J. Cava, E. Kaxiras, H.-Z. Lu, H. Lin, L. Fu, N. Gedik *et al.*, *Nature (London)* **565**, 337 (2018).
- [28] K. Kang, T. Li, E. Sohn, J. Shan, and K. F. Mak, *Nat. Mater.* **18**, 324 (2019).
- [29] O. O. Shvetsov, D. V. Esin, A. V. Timonina, N. N. Kolesnikov, and E. V. Deviatov, *JETP Lett.* **109**, 715 (2019).
- [30] M.-S. Qin, P.-F. Zhu, X.-G. Ye, W.-Z. Xu, Z.-H. Song, J. Liang, K. Liu, and Z.-M. Liao, *Chin. Phys. Lett.* **38**, 017301 (2021).
- [31] S. Dzsaber, X. Yan, M. Taupin, G. Eguchi, A. Prokofiev, T. Shiroka, P. Blaha, O. Rubel, S. E. Grefe, H. H. Lai, Q. Si, and S. Paschen, *Proc. Nat. Acad. Sci.* **118**, e2013386118 (2021).
- [32] D. Kumar, C. H. Hsu, R. Sharma, T. R. Chang, P. Yu, J. Wang, G. Eda, G. Liang, and H. Yang, *Nat. Nanotechnol.* **16**, 421 (2021).
- [33] K. Hamamoto, M. Ezawa, K. W. Kim, T. Morimoto, and N. Nagaosa, *Phys. Rev. B* **95**, 224430 (2017).
- [34] Y. Araki, *Sci. Rep.* **8**, 1 (2018).
- [35] M. Papaj and L. Fu, *Phys. Rev. Lett.* **123**, 216802 (2019).
- [36] D. Mandal, K. Das, and A. Agarwal, *Phys. Rev. B* **102**, 205414 (2020).
- [37] S. K. Das, T. Nag, and S. Nandy, *Phys. Rev. B* **104**, 115420 (2021).
- [38] C. Zeng, S. Nandy, and S. Tewari, *Phys. Rev. Res.* **2**, 032066(R) (2020).
- [39] X.-Q. Yu, Z.-G. Zhu, J.-S. You, T. Low, and G. Su, *Phys. Rev. B* **99**, 201410(R) (2019).
- [40] C. Zeng, S. Nandy, A. Taraphder, and S. Tewari, *Phys. Rev. B* **100**, 245102 (2019).
- [41] C. R. Woods, L. Britnell, A. Eckmann, R. S. Ma, J. C. Lu, H. M. Guo, X. Lin, G. L. Yu, Y. Cao, R. V. Gorbachev, A. V. Kretinin, J. Park, L. A. Ponomarenko, M. I. Katsnelson, Y. N. Gornostyrev, K. Watanabe, T. Taniguchi, C. Casiraghi, H. J. Gao, A. K. Gemi *et al.*, *Nat. Phys.* **10**, 451 (2014).
- [42] G. W. Semenoff, *Phys. Rev. Lett.* **53**, 2449 (1984).
- [43] E. McCann and V. I. Fal'ko, *Phys. Rev. Lett.* **96**, 086805 (2006).
- [44] M. Mucha-Kruczyński, I. L. Aleiner, and V. I. Fal'ko, *Phys. Rev. B* **84**, 041404(R) (2011).
- [45] M. Koshino and T. Ando, *Phys. Rev. B* **76**, 085425 (2007).
- [46] J. Xu, W. A. Phelan, and C.-L. Chien, *Nano Lett.* **19**, 8250 (2019).
- [47] K. Uchida, S. Takahashi, K. Harii, J. Ieda, W. Koshibae, K. Ando, S. Maekawa, and E. Saitoh, *Nature (London)* **455**, 778 (2008).